Biophysical Characterization of a Novel Enzyme Family

By

XIAOQING HUANG

THESIS

Submitted in partial satisfaction of the requirements for the degree of

MASTER OF SCIENCE

in

Pharmaceutical Chemistry

in the

OFFICE OF GRADUATE STUDIES

of the

UNIVERSITY OF CALIFORNIA

DAVIS

Approved:

Justin Siegel, Chair

Dean Tantillo

Philipp Zerbe

Committee in Charge

2022

ACKNOWLEDGMENTS

I would like to thank everyone that make my academic career and this master's degree possible. First, I would like to extend my deepest gratitude to my family, who have always supported me throughout the past 20 years of study. They always show their love and kindness when I was stressed, and they helped me get through all the hard times.

I would also like to express my gratitude to all members of the Siegel Lab, especially Dr. Justin Siegel. Dr. Siegel provided many interesting ideas and a great opportunity for me to learn how to be a qualified scientist. We all experienced research challenges during the pandemic, but we excelled in collaboration. All of my lab mates were very supportive. They helped me with challenges and trained me, allowing me to become an independent researcher. It was my pleasure to be a part of the Siegel Lab.

DEDICATION

I dedicate this work to my parents, Yongqin Huang and Limei Zheng, and my brother, Zifeng Huang. They have supported me through my whole academic life, and I wouldn't have gotten here without their love and support. I also want to dedicate this work to everyone who contributed their knowledge and effort during the global pandemic.

ABSTRACT OF THE THESIS

Biophysical Characterization of a Novel Enzyme Family

By

Xiaoqing Huang

Master of Science, Graduate Program in Pharmaceutical Chemistry
University of California, Davis, September 2022
Dr. Justin Siegel, Chairperson

Enzymes, which act as catalysts for specific bioreactions under unique conditions, are valuable biological macromolecules that were originally found in living organisms. With the changing environment, some organisms have evolved differently to adapt to new environment conditions. However, not all organisms can overcome environmental stress, which results in the loss of enzyme activity. Thus, in this thesis, I first study soluble starch synthase I in wheat, which is largely affected by global climate change and causes a worldwide reduction in wheat yield. The first chapter characterizes the thermostability of 18 soluble starch synthase I enzymes from different crops, and through a thermal inactivation assay, identifies a more thermostable soluble starch synthase I compared to wheat. The results of this chapter can be applied for future genome editing to improve starch yield in wheat under high-temperature conditions.

In addition, exploring the application of enzymes and applying it to our daily lives could largely be beneficial to humans' daily applications. Many enzymes have been used in manufacturing for production or biodegradation. Therefore, the second chapter explores the application of carboxylic acid reductase and aldehyde-deformylating oxygenase in the biodegradation of perfluorooctanoic acid. The substrate promiscuity of carboxylic acid reductase was studied by measuring its kinetic parameters against different substrates.

TABLE OF CONTENTS

LIST OF TABLES

LIST OF FIGURES

INTRODUCTION

As natural catalysts, enzymes are responsible for many specific bioreactions in nature. [1] However, the environmental conditions in their habitat changes over time, which puts pressure on enzymes, resulting in adaption to new environments. [2] As a result, many neutral mutations within an enzyme aim to improve their fitness in an environment while maintaining their behavior. [3] Though most mutations that happen under selective pressure are detrimental to individual fitness, mutations that are carried to the next generation can have a beneficial impact. [4] The evolution of enzymes can be studied through enzyme characterization, and enzymes can be designed to have desired physical or chemical properties. [5,6] There are many methods or parameters that have been used to characterize enzyme properties, such as kinetic stability, thermodynamic stability, and substrate specificity. [7,8] The characterization of enzymes provides a fundamental dataset for downstream protein studies and engineering. Evolution also opens the door to enzyme promiscuity, which maybe not contribute to enzyme itself fitness in the environment but can increase the fitness of the organism through chemical diversity. [9] Recently, enzyme promiscuity is receiving increasing attention since it not only provides a starting point for scientists to discover non-biological functions for enzymes, but also can be used for protein engineering studies on the evolution of enzyme mechanisms. [10–12] Therefore, it is of interest to explore enzyme promiscuity, which will maximize the application of enzymes to the increasing human demand. Overall, this thesis is going to study the evolution impact on enzymes through characterization, which aims to provide fundamental information for improving enzyme activity and expanding enzyme application in the future.

CHAPTER 1: CHARACTERIZATION OF 18 SOLUBLE STARCH SYNTHASE I FROM DIFFERENT CROPS

1.1 INTRODUCTION

Wheat (*Triticum aestivum L*) is one of the world's most cultivated grain crops, occupying approximately 40% of nutrients in daily human consumption. [13] However, the increasing global temperature has negatively impacted wheat yield. Elevated temperature causes a reduction of starch deposition during the grain filling stage, resulting in loss of overall crop weight. [14] A previous study has reported that wheat's optimum temperature for starch deposition during the grain filling stage is 15–22°C. [15] Every 1°C that exceeds the optimum temperature will cause a reduction in yield by 3 to 4%. [16] A short period of heat stress can also reduce the grain number and individual grain sizes. [17]

Starch is composed of two major forms of polysaccharides: amylose and amylopectin. [18] Amylose is a linear polysaccharide composed of glucose units through glycosidic bonds. Amylopectin, which composes ~80% of the total starch components, is a highly branched polymer synthesized from amylose. [18,19] The synthesis of amylose and amylopectin in higher plants is controlled by starch synthase (1,4-D-glucan-4-α-D-glucosyltransferase), which belongs to glycosyltransferase family 5 (GT5). [20] At least five classes of starch synthase have been identified in plants, including granule-bound starch synthase (GBSS) and soluble starch synthase (SSSI-IV). [21] All starch synthases catalyze the same reaction: adding glucose from ADP-glucose to the non-reducing end of the growing maltooliosaccharide through an α-1,4-glycosidic bond. [22] (Figure 1-1) Each class has different substrate specificity and physiochemical properties, conferring a unique role along the starch biosynthesis pathway. [23] Of the soluble starch synthase classes, soluble starch synthase I (SSSI) is the class with only one isoform, and they are involved

in the early stage of the amylose production process. [24] SSSIs preferentially use smaller glucose chains as substrates and only elongate substrates to medium-length (8–12 degrees of polymerization). [23] When glucose chains are elongated to a certain length, SSSIs will become a relatively inactive enzyme in the granule. [25] SSSIs occupy over 70% of the starch synthesis activity within the soluble fraction of rice. [26] As a result, SSSI is considered an essential enzyme in the plant starch synthesis process, which determines the efficiency of follow-up reactions performed by other soluble starch synthases.

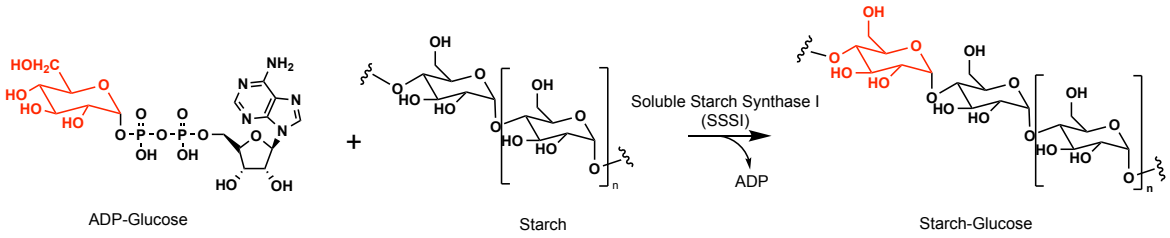

Figure 1-1: The reaction that soluble starch synthase I (SSSI) catalyzes in the plant. ADP-glucose serves as the substrate, and glucose is transferred to the growing glucose chain (starch) through an α -1,4-glycosidic bond, and ADP is released.

However, a previous study showed that SSSI is the most heat-sensitive enzyme among the soluble starch synthase family. [15] SSSI has a low optimum temperature (25°C), and enzymatic activity decreases when the temperature is over 30°C, which reduces the overall rate of starch synthesis during the grain filling stage. [27–29] Dr. Harold Trick from Kansas State University successfully improved the wheat grain yield under heat stress by expressing a more thermostable soluble starch synthase gene in transgenic wheat, and the kernel weight increased by over 20% compared to non-transgenic wheat under heat stress conditions. [15]

In addition to SSSIs from rice, other viable SSSIs have been found in crops that typically grow under high temperature conditions. By characterizing the thermostability of their SSSIs, a valuable thermostability database for SSSIs can be obtained, which would be

helpful for future enzyme design. [30] As a result, we choose 17 SSSIs from other crops to compare to the SSSIs from wheat (*Triticum aestivum L*). The SSSIs were selected from crops that typically grow in higher temperature environments compared to wheat. They share high sequence similarity, with an average pairwise sequence identity of 68% (Figure 1-2). The main goal of this study was to characterize the thermostability of 18 SSSIs from different crops (originally grown at high temperature) and provide a valuable database of thermostable SSSI sources.

In this study, we cloned 18 SSSIs DNA fragments that have been optimized for transformation into an *Escherichia coli* (*E. coli*) pET29b+ vector. The proteins were produced through auto-induction and purified through immobilized metal affinity chromatography. Enzyme kinetic stability was measured using a thermal inactivation (T_{50}) assay, a parameter used to measure the temperature when enzyme activity is reduced by 50% after heat treatment for a certain amount of time.

1.2 MATERIALS AND METHODS

1.2.1 Plasmid collection and Gibson Assembly

Collaborators (Dr. Harold and TechAccel) provided SSSI genes from 18 different crops. The abbreviation for genes and the phylogenetic tree are shown in Figure 1-2. The DNA sequences that had been codon optimized for *E. coli* were cloned into a pET29b+ vector through Gibson assembly, [31] and the recombinants were verified through Sanger sequencing. [32]

Gene Name	Abbriviation
Triticum aestivum L	*Ta*SSI*(*1)
Triticum aestivum L	*Ta*SSI(2)
Oryza sativa	*Os*SSI
Hordeum vulgare	*Hv*SSI
Vitis vinifera	*Vitvi*SSI
Zea mays	*Maize*SSI
Manihot esculenta	*Manes*SSI
Arabidopsis thaliana	*Arath*SSI
Glycine Max	*Glyma*SSI
Amaranthus Cruentus	*Amacr*SSI
Aegilops Tauschii	*Aegta*SSI
Phaseolus Vulgaris	*Phavu*SSI
Sorghum bicolor	*Sorbi*SSI
Prunus Persica	*Prupe*SSI
Popiar Triocarpa	*Poptr*SSI
Solanum lycopersicum	*Sollc*SSI
Cicer Artetinum	*Cicar*SSI
Theobroma Cacao	*Thecc*SSI

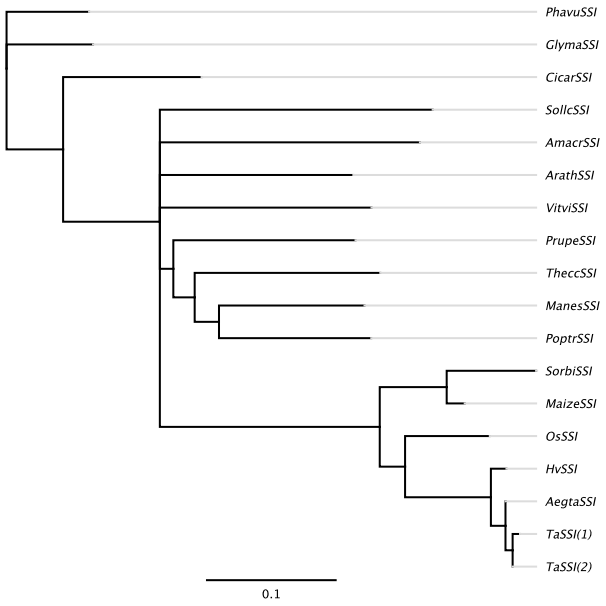

Figure 1-2: A table of the 18 genes selected in this study and their abbreviation. The phylogenetic tree was generated using Geneious. [33] The distance scale is 0.1.

1.2.2 Plasmid transformation and protein production

Once the sequences were verified, the plasmids were transformed into electrocompetent *E. coli* BLR(DE3) cells through electrophoresis. Terrific Broth (TB) (200 µl) was added and shaken at 37ºC for 1 hour. The cells were then plated onto a Lysogeny Broth (LB) agarose plate with kanamycin selection. The plate was incubated at 37ºC overnight. A single colony was selected and grown in 5 mL of TB media overnight with 1 mM kanamycin and 1 mM tetracycline in 50 mL falcon tubes with breathable tape. The whole volume was transferred into 500 mL TB sub-cultures containing 1 mM kanamycin and 1 mM $MgSO_4$ for overnight incubation. The sub-culture was shaken at 37ºC overnight, and the cell pellet was collected by centrifuging at 4,700 rpm for 10 minutes. The cell pellet was resuspended in 500 mL induction TB media with 1x 5052, 1x NPS, 0.5% glucose, 1 mM kanamycin, and 1 mM $MgSO_4$. [34,35] The induction media was incubated at

18ºC for 24 hours, and the cell pellet was collected by centrifuging at 4,700 rpm for 10 minutes. The collected cell pellets were resuspended in 25 mL wash buffer (20 mM Tris-HCl, pH=8, 200 mM NaCl, 10 mM imidazole, 10% glycerol) before being frozen at -20ºC for downstream purification.

1.2.3 Protein purification

After thawing the resuspended cell pellet, the cells were lysed with 1 mM DNase, 1 mM PMSF, and 1 mM lysozyme in the wash buffer, followed by sonication for 30 seconds on and 30 seconds off with an amplitude of 60 for a total of two and half minutes. The lysis mixture was then clarified by centrifugation at 4,700 rpm for one and half hours. The lysate was transferred into a 15 mL immobilized metal ion chromatography column loaded with 1 mL of 50% cobalt resin slurry. Once the lysate had flowed through, 15 mL of wash buffer was added five times to wash the bed of the beads. The protein could be eluted with 1.4 mL wash buffer with 200 mM imidazole after all the wash went through the column. The final concentration of the protein was determined by absorbance at 280 nm. Proteins were considered to have expressed successfully by the presence of a band on 4–12% sodium dodecyl sulfate-polyacrylamide gel electrophoresis (SDS-PAGE) from Life Technologies, which was run at approximately 75 kD.

1.2.4 Thermo Inactivation (T_{50}) Assay

A coupled T_{50} assay was conducted following the methods described in a previous study (Figure 1-3). [36] Briefly, the coupled reaction consisted of three steps. SSSI catalyzed the first reaction of transferring the glucose to the glycogen (acceptor), followed by the loss of ADP. ADP and phosphoenolpyruvate (PEP) become substrates for the second reaction, which was catalyzed by pyruvate kinase (PK). The products for the second reaction were pyruvate and ATP, and pyruvate was the substrate in the third reaction. The third reaction was catalyzed by lactate

dehydrogenase (LDH), which transferred the hydrogen from NADH to pyruvate, forming lactate. The reduction of NADH was monitored using a spectrometer at 340 nm, which allowed for the monitoring of SSSI activity. [36]

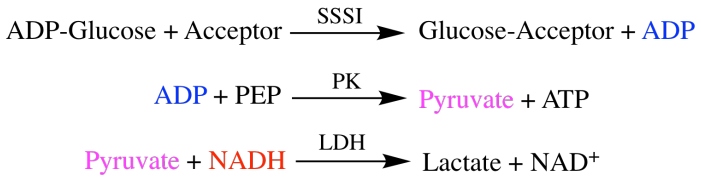

Figure 1-3: The reaction scheme for the SSSI T_{50} assay. Acceptor: Glycogen; PEP: phosphoenolpyruvate; PK: Pyruvate kinase; LDH: Lactate dehydrogenase. The activity of SSSI is determined by the reduction of NADH, which is monitored through a spectrometer at 340 nm. [36]

Purified proteins were diluted in the wash buffer with an enzyme concentration of 0.01–0.1 mg/mL. Diluted enzymes were then aliquoted in triplicate into 96-well non-skirted PCR plates, and each well contained 30 µL of diluted enzymes. Proteins were thermally challenged at ten different temperatures (50ºC, 45.7ºC, 42.4ºC, 37.7ºC, 33.6ºC, 31.3ºC, 30ºC, 25ºC, 20ºC, 15ºC) for one hour in the thermal cycler (BioRad). The reaction mix (50 mM Bicine pH 8.5, 25 mM potassium acetate, 2 mM $MgCl_2$, 10 mM reduced DTT, 0.375 mM NADH, 0.7 mM phosphoenolpyruvate tri-cyclohexylammonium salt, 6 U ml^{-1} pyruvate kinase, 30 U ml^{-1} lactate dehydrogenase) was prepared and kept on ice when the incubation nearly finished. In total, 10 µL of 5 mM ADP-Glucose was aliquoted into each well of the 96-well non-binding assay plate, followed by the addition of 80 µL reaction mix. Immediately after the heat treatment, 10 µL of heat-treated protein was transferred into the prepared 96-well non-binding assay plate. The blank control was prepared with GFP. The spectrometer plate reader (Synergy) monitored the reduction of NADH at an absorbance of 340 nm. The assay was done in triplicate, and the enzyme reaction rate at the temperature heat treatment was calculated using the Data Reduction function on Gen5™ 2.09. [37] The blank was subtracted from the experimental data. The average of triplicated data was

fitted into both a linear regression and sigmodal equation. T_{50} was calculated from both equations, and that with a lower standard deviation was shown herein. Meanwhile, the specific activity of each activated enzyme were calculated from the 100% enzyme activity.

1.3 RESULTS AND DISCUSSION

1.3.1 SSSI sequence similarity

The average pairwise sequence similarity of the 18 SSSIs was 68% (Figure 1-4). The high sequence conservation among the SSSIs suggests that they have a unique and specific role in the amylopectin biosynthesis pathway.

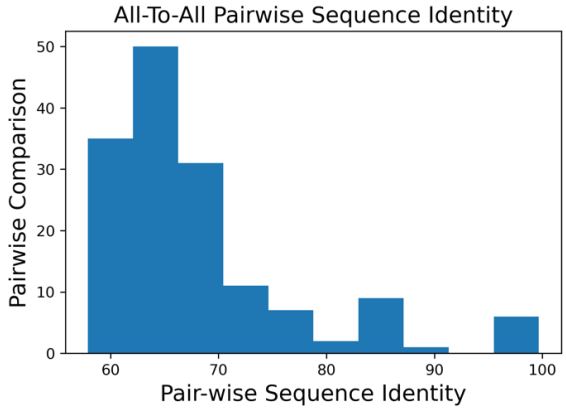

Figure 1-4: All-to-all sequence identity pairwise comparison. Eighteen tested SSSI has approximately 68% of sequences identity.

1.3.2 Protein yield and SDS-PAGE

The concentration of each SSSI was determined by the UV absorbance at 280 nm. The purity of the protein was validated through SDS-PAGE. The gel image is shown in Figure 1-5. Protein bands near 75 kD indicate the successful expression of SSSIs. The molecular mass of each SSSI was calculated from their sequences by using Expasy. [38] The detailed molecular weight of each SSSI is listed in Table 1-1. SSSIs with clear, present bands at their corresponding molecular weight were chosen for the subsequent thermal inactivation assay: *Ta*SSI(1), *Ta*SSI(2), *Hv*SSI, *Vitvi*SSI, *Maize*SSI, *Manes*SSI, *Glyma*SSI, *Sorbi*SSI, *Poptr*SSI, *Sollc*SSI, *Ageta*SSI, and

*Phavu*SSI. The expression results were based on the enzymatic activity. Bands were present in lower molecular weight regions, which may be from background contamination with other enzymes during the protein production process. Therefore, the A280 measurements likely overestimated the intreated protein in the final product. There is an additional band with the SSSIs, which may be a result of protein degradation.

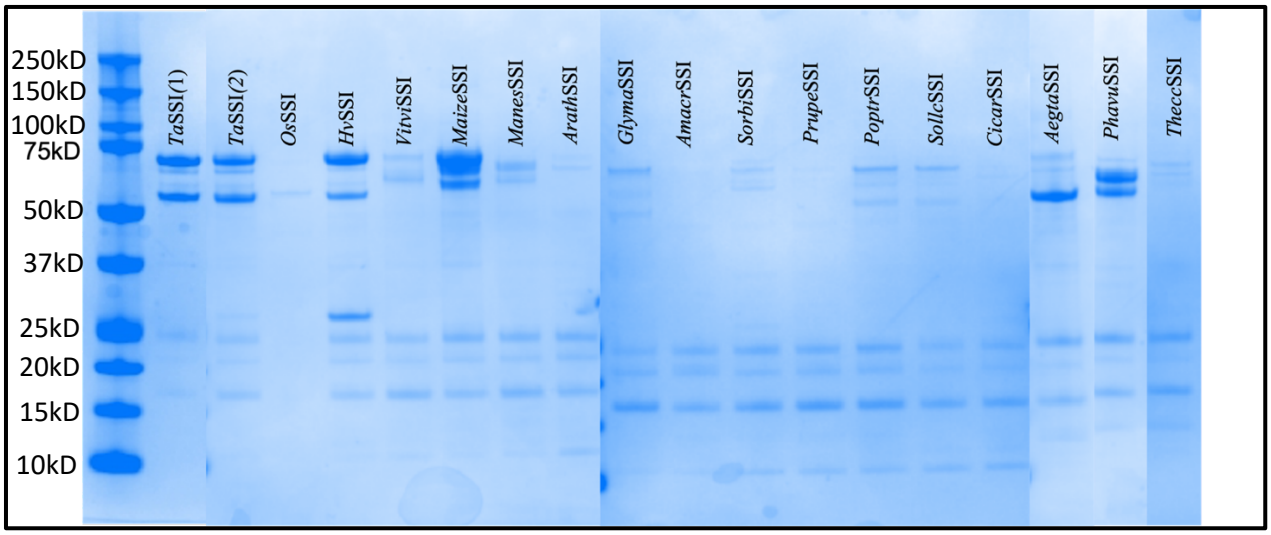

Figure 1-5: The SDS-PAGE image for 18 SSSI. The molecular weight for SSSIs ranges from approximately 63 kD to 72 kD. Details of molecular weight for each SSSI can be found in Table 1-1.

1.3.3 Discussion of T_{50} Findings

The enzymatic activity of SSSIs ranged from 15°C to 50°C, and this study considered the highest activity of 100% residual activity (Figure 1-6). The T_{50} values were calculated from 100% residual activity to the lowest activity recorded. Column A in Figure 1-6 shows the results of the enzyme activity analysis at all tested temperatures. Column B shows the regression lines of the T_{50} calculation as well as the corresponding T_{50} values in the top right corner.

A total of 10 out of 18 tested SSSIs showed enzyme activity. Four (*Ta*SSI(2), *Vitvi*SSI, *Glyma*SSI, *Poptr*SSI) out of those ten SSSIs showed the highest activity (100% residual activity) below 30°C. *Hv*SSI had the highest activity at the highest temperature (37.7°C) compared with all

SSSIs. In addition to *Hv*SSI and *Phavu*SSI, other SSSIs showed a linear decrease in activity with the increasing temperature. Activity was halted in all SSSIs at 50°C. Wheat SSSIs (*Ta*SSI(1) and *Ta*SSI(2)) had relatively low T_{50}, which were 37.27°C and 34.69°C, respectively. *Glyma*SSI and *Poptr*SSI had similar T_{50} compared to wheat. Six (*Hv*SSI, *Vitvi*SSI, *Maize*SSI, *Aegta*SSI, *Phavu*SSI, and *Sollc*SSI) SSSIs had a T_{50} above 40°C, and *Vitvi*SSI had the highest T_{50} (46.48°C) among all SSSIs; it higher than the T_{50} of wheat by approximately 10°C. The T_{50} for *Ta*SSI(1) showed that every 1°C exceeding 30°C caused an average decrease of 7% in *Ta*SSI(1) activity. This was also observed in *Phavu*SSI and *Hv*SSI. Even though *Vitvi*SSI was the most active at the lowest temperature (15°C), it had the highest T_{50} (46.48°C), indicating that every 1°C increase in temperature would cause less than a 2% decrease in enzyme activity. Other SSSIs showed a decrease in activity by 3–5% with every 1°C increase in temperature. The specific activity of all SSSIs are summarized in Table (1-1). *Ta*SSI(1) had the highest specific activity, at least two times higher than any other SSSI.

When the enzyme activity was screened at temperature of 15–50°C (Figure 1-6, column A), the results of *Hv*SSI, *Maize*SSI, *Phavu*SSI, *Sollc*SSI, and *Aegta*SSI had a large difference in activity between 25°C and 30°C, which might be due to instrumental error because the BioRad PCR machine used only allowed the temperature gradient to be set within a specific range. The most suitable temperature gradient should therefore be 30–50°C. Thus, the enzyme activity assay was performed separately for 15-30°C and 30-50°C, but the same experimental conditions were followed.

The temperature dependence of SSSIs is evident in these findings. The results from *Ta*SSI(1) confirmed that SSSI from wheat is the most thermal sensitive SSSI included in this study. *Vitvi*SSI is potentially the most thermostable SSSI in this study because had the highest T_{50} and its

activity was least affected the temperature. *Vitvi*SSI, which is from *Vitis vinifera* (European grapevine), grow in warm climates where the temperature may exceed 40°C during the summer. [39] This indicates that SSSIs in crops that primarily grow in warm climates are potentially more heat resistant than those from crops grown in cold climates. However, exact phycological conditions of SSSI activity were not able to be recreated in this study. This assay only focused on the activity of SSSIs *in vitro*, and it did not account for possible protein–protein interactions within the plant, potentially improving SSSI activity. For example, the interaction between SSSIs and soluble branch enzymes (SEBs) would stimulate SSSI activity. [40] In addition, glycerol in the wash buffer originally intended to stabilize SSSI would increase SSSI stability during the assay.

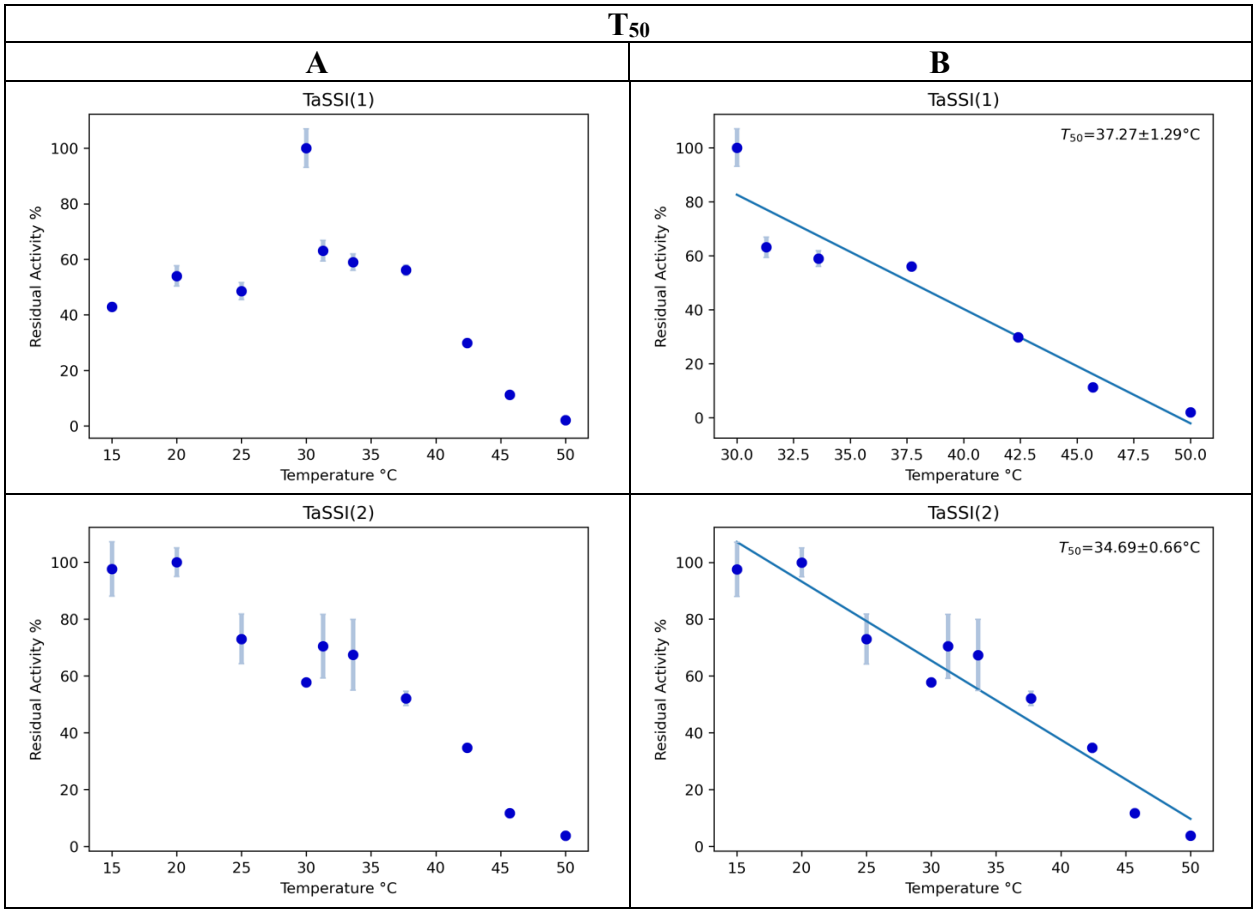

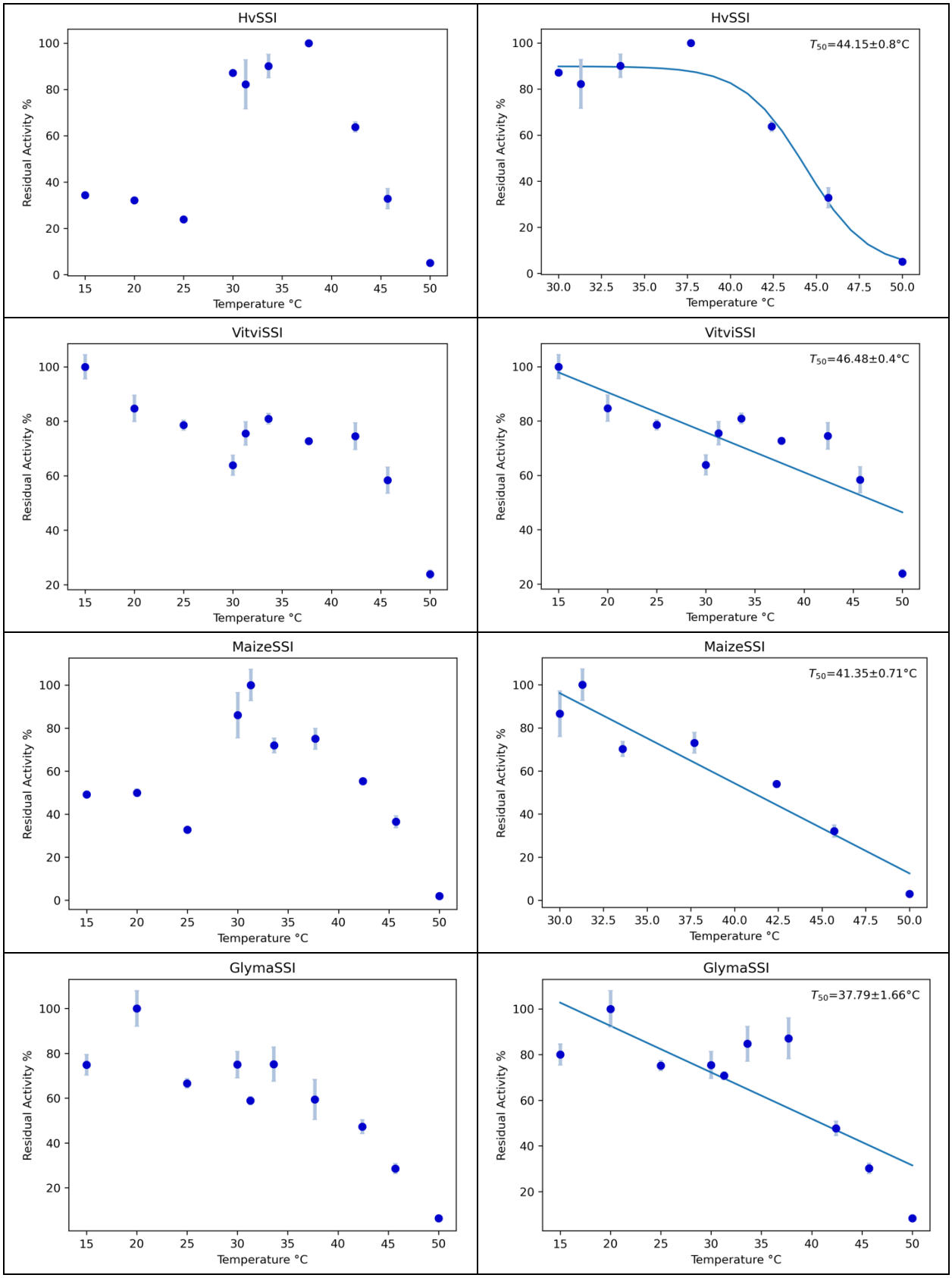
HvSSI
Residual Activity %
Temperature °C
HvSSI
T_{50}=44.15±0.8°C
Residual Activity %
Temperature °C
VitviSSI
Residual Activity %
Temperature °C
VitviSSI
T_{50}=46.48±0.4°C
Residual Activity %
Temperature °C
MaizeSSI
Residual Activity %
Temperature °C
MaizeSSI
T_{50}=41.35±0.71°C
Residual Activity %
Temperature °C
GlymaSSI
Residual Activity %
Temperature °C
GlymaSSI
T_{50}=37.79±1.66°C
Residual Activity %
Temperature °C

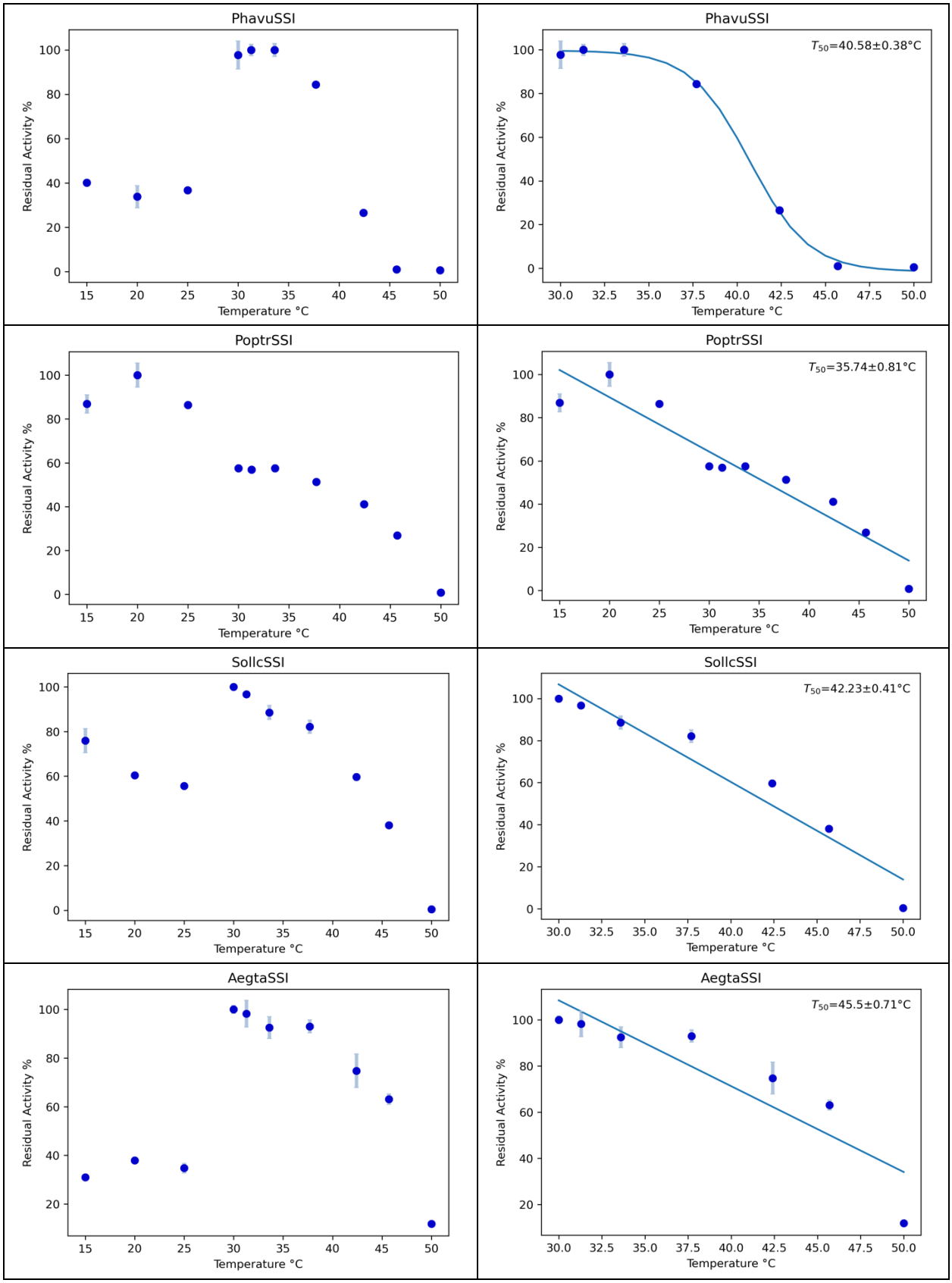
PhavuSSI
Residual Activity %
Temperature °C
PhavuSSI
T_{50}=40.58±0.38°C
Residual Activity %
Temperature °C
PoptrSSI
Residual Activity %
Temperature °C
PoptrSSI
T_{50}=35.74±0.81°C
Residual Activity %
Temperature °C
SollcSSI
Residual Activity %
Temperature °C
SollcSSI
T_{50}=42.23±0.41°C
Residual Activity %
Temperature °C
AegtaSSI
Residual Activity %
Temperature °C
AegtaSSI
T_{50}=45.5±0.71°C
Residual Activity %
Temperature °C

Figure 1-6: T_{50} data from 10 SSSIs. Column A shows SSSI activity at temperatures ranging from 15ºC to 50ºC. Column B shows the regression line used to calculate T_{50}. Each was fitted onto both linear regression and sigmodal regression equations starting from the 100% residual activity. The T_{50} values are shown on the top right corner, and they indicate the temperature at which the residual activity lost 50% after 1 hour of incubation. In all graphs, the x-axis shows the incubation temperature in ºC, and the y-axis shows the residual activity in %. The data on the graph are the average of at least two datasets, and the error bars represent the standard error.

Table 1-1: Soluble starch synthase I (SSSI) gene names, their corresponding abbreviation used in this study, and UniProt IDs. The molecular weight for each SSSI is shown in kD. Table summarizes the expression (mg/mL) from protein production and T_{50} values from a thermal inactivation study for all expressed SSSI. "-" represents no expression and no activity observed in this study.

Gene Name	Abbreviation	UniProt ID	Molecular weight (kD)	Expression (mg/ml)	T_{50} (ºC)	Specific Activity x10^4 (unit/mg)
Triticum aestivum L	*Ta*SSI(1)	Q9SQG9	71.03	0.018	37.27±1.29	8.43
Triticum aestivum L	*Ta*SSI(2)	Q9SQG9	68.08	0.047	34.69±0.66	1.90
Oryza sativa	*Os*SSI	Q0DEC8	68.98	-	-	-
Hordeum vulgare	*Hv*SSI	Q9M5A3	68.59	0.045	44.15±0.8	4.08
Vitis vinifera	*Vitvi*SSI	F6H795	69.83	0.042	46.48±0.4	1.93
Zea mays	*Maize*SSI	O49064	67.71	0.026	41.35±0.71	4.97
Manihot esculenta	*Manes*SSI	B3SRP2	67.15	-	-	-
Arabidopsis thaliana	*Arath*SSI	Q9FNF2	63.41	-	-	-
Glycine max	*Glyma*SSI	I1JYR0	70.26	0.071	37.79±1.66	1.36
Amaranthus cruentus	*Amacr*SSI	G9M933	69.82	-	-	-
Aegilops Tauschii	*Aegta*SSI	Q9SQH0	68.92	0.06	45.5±0.71	3.3
Phaseolus vulgaris	*Phavu*SSI	Q75T80	68.65	0.053	40.58±0.38	2.64
Sorghum bicolor	*Sorbi*SSI	Q9SBL2	65.87	-	-	-
Prunus persica	*Prupe*SSI	M5X7A6	69.2	-	-	-
Poplar triocarpa	*Poptr*SSI	A0A2K1XGC4	71.63	0.1	35.74±0.81	1.12
Solanum lycopersicum	*Sollc*SSI	K4BI85	70.05	0.09	42.23±0.41	1.34

Cicer artetinum	*Cicer*SSI	A0A1S2YD89	69.51	-	-	-
Theobroma cacao	*Thecc*SSI	A0A061G1W2	73.07	-	-	-

1.4 CONCLUSIONS AND RECOMMENDATIONS

Wheat yields have decreased with the increasing global temperature. SSSI, which has been defined as the most heat-sensitive enzyme in the starch synthesis pathway, has thus been frequently studied in an attempt to improve wheat yield. [28,29] A possible way to improve the thermostability of SSSI in wheat through genetic modification has been identified and finding a more thermostable SSSI than wheat through thermostability characterization will be useful for future enzyme engineering. [15]

Thus, we selected 18 SSSI enzymes for comparison. After transformation, protein expression and purification, 10 out of 18 showed enzymatic activity. T_{50} was used to characterize the thermostability for all SSSIs. Six SSSIs had higher T_{50} values compared to wheat SSSIs. *Vitvi*SSI is the overall best candidate because its activity was the least affected by the increasing temperature. This study provides a detailed data bank of SSSI thermal stability, providing the groundwork for future studies on increasing SSSI thermostability in wheat and therefore improving wheat yield under high temperature conditions. However, this study did not account for the physiological conditions of SSSIs, which might contribute to their thermostability in the plant. Future studies should repeat the enzyme activity test between 15–30℃, which can essentially eliminate experimental and instrumental errors. In addition, it might be interesting to examine SSSIs from different wheat lines in future study, which might allow for using breeding for crop improvement.

CHAPTER 2: BIOPHYSICAL CHARACTERIZATION OF CARBOXYLIC ACID REDUCTASE WITH PERFLUOROOCTANOIC ACID

2.1 INTRODUCTION

Carboxylic acid reductase (CAR), also known as aryl-aldehyde oxidoreductase, can reduce a wide range of aromatic and aliphatic carboxylic acids into their corresponding aldehydes with the co-factors of ATP and NADPH. [41] Because of the regioselective reduction of carboxylic groups and non-toxic and mild reaction conditions, CARs are widely used in industry. [42] CAR can provide an alternative enzymatic synthesis pathway for reactive aldehyde products, which is favorable given the increasing demand for "green" chemistry manufacturing. [43] CAR is an attractive enzyme for various cascade reactions in which aldehydes are the essential building blocks for the synthesis. [44] One of the enzyme cascades that has received growing attention involves CAR and aldehyde-deformylating oxygenases (ADOs). ADOs is an enzyme family that catalyzes medium to long-chain aldehydes into alkanes, with the carbonyl group leaving as formate. [45] The CAR and ADO reaction cascade has been engineered for renewable biofuel production, which provides a possible sustainable energy solution for our continued reliance on fossil fuels. [43,46]

Recently, highly fluorinated compounds released into biological systems by industries are gaining increasing attention worldwide. [47–49] Perfluoroalkyl acids (PFAS) are a group of artificial chemicals produced by industry since the 1940s. Because PFAS have surfactant properties, such as water resistance, stain resistance, and oil resistance, they are widely used for coating clothing fabric, carpets, and food packaging. [50] A commonly used PFAS is perfluorooctanoic acid (PFOA), an eight-carbon fluorinated compound attached by a carboxylic acid functional group. Before 2004, the global production of the PFOA was approximately 1,200 metric tons per year. [51] Since PFOA

accumulates in the environment and is difficult to degrade, the U.S Environmental Protection Agency initiated the PFOA Stewardship Program in 2006, which required major companies to reduce the use of PFOA in their production on a global basis by 95% no later than 2010. [51] Evidence shows that PFOA can accumulate in the human body and cause health problems such as liver damage and kidney cancer [52]. Therefore, it is urgent to degrade the existing PFOA in the environment. Since carbon-fluorine bonds are considered the strongest bonds in organic chemistry, some methods, such as activated carbon filtration, reverse osmosis, and ion exchange, require high temperature and high pressure, which make them impractical for *in situ* treatment. [51,53] Some studies have demonstrated that PFAS can be degraded through photooxidation and photocatalytic ozonation with ZnO assistant. [54,55] However, although these methods showed over 70% efficiency for PFOA degradation, they are hard to use on a large scale. Moreover, biodegradation is considered a more accessible and eco-friendly way to remove organic environmental pollutants in the water and soil. A recent study showed that PFOA could be biodegraded in the bacterium *Acidimicrobium sp*. strain A6, and the successful biodegradation of PFOA was determined by the formation of fluoride in the enriched culture. [56] However, the final product of PFOA degradation in a whole cell assay is challenging to identify because numerous enzymes can interfere with the quantification. [56] Therefore, the use of purified enzymes to degrade PFOA *in vitro* is a better way to determine biodegradation, which is limited in current research. [57]

To date, no purified enzyme has been characterized for degrading PFOA. Fortunately, a proposed mechanism of PFOA degradation has been published. [58] The overall mechanism is a consecutive one-carbon chain shortening cycle, which can be achieved by using one or more enzymes. Based on previous research, a key intermediate is a carbon-centered radical, which precedes a chain shortening reaction with the help of oxygen species and water molecules. [58]

This study modified the reaction cascade of CAR and ADO to perform this biodegradation mechanism for PFOA. The enzymatic mechanisms of CAR and ADO are well known and can theoretically accomplish the proposed biodegradation pathway of PFOA (Figure 2-1). A CAR from *Mycobacterium marinum* (*mm*CAR) was selected as a candidate since it can convert a broad range of fatty acids (from C_4 to C_{18}) into their corresponding aldehyde. [43] The aldehyde product will then become a substrate for ADO, and the reaction will continue with consecutive one-carbon chain shortening cycles.

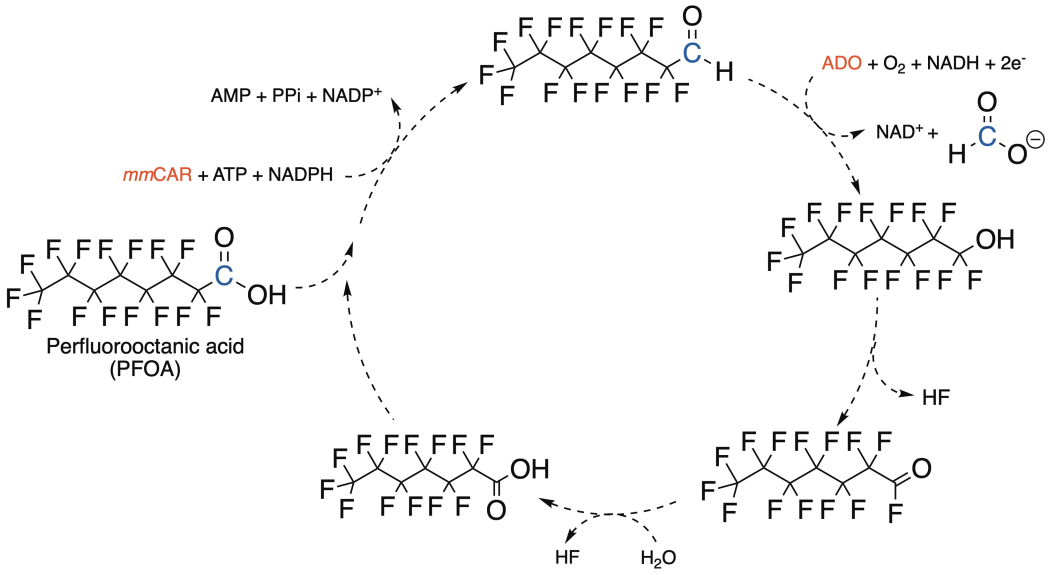

Figure 2-1: The proposed mechanism for the perfluorooctanoic acid (PFOA) degradation pathway with carboxylic acid reductase (CAR) and aldehyde-deformlating oxygenase (ADO). The reaction starts with *mm*CAR reducing PFOA into its corresponded aldehyde with the co-factors of ATP and NADPH. Then, ADO catalyzes the aldehyde product into difluoro alcohol with carbonyl left as formate, which spontaneously eliminates HF and form acyl-fluoride. Then, water hydrolyzes acyl-fluoride to form a new fluoro-carboxylate that is one carbon shorter, which is a starter substrate for the next reaction cycle. The cycle will repeat, leading to complete degradation.

Before performing the CAR-ADO reaction cascade *in vitro,* it is necessary to validate the enzymatic activity of *mm*CAR with PFOA and the mechanism of the reaction. The mechanism of the CAR catalytic pathway has been well studied and is performed by three domains: the adenylation, thiolation, and reduction domains. [41] The proposed mechanism consists of four main

steps with the assistance of two co-factors: ATP and NADPH (Figure 2-2). [59] The effect of electron density on aryl-substituted carboxylic substrates has been investigated with a known native substrate of CAR, a benzoic acid. Previous experiments have shown that an electron-donating group located at the para and meta position could drive the electron into the pi system and make the first nucleophilic attack more favorable. [59] However, there are limited studies focused on enzyme substrate specificity on substituted fatty acid substrates, especially concerning the effect of electron density when next to a carboxylic acid. Nevertheless, enzymatic promiscuity needs to be further studied; thus, this study investigated the substrate specificity for CAR activity.

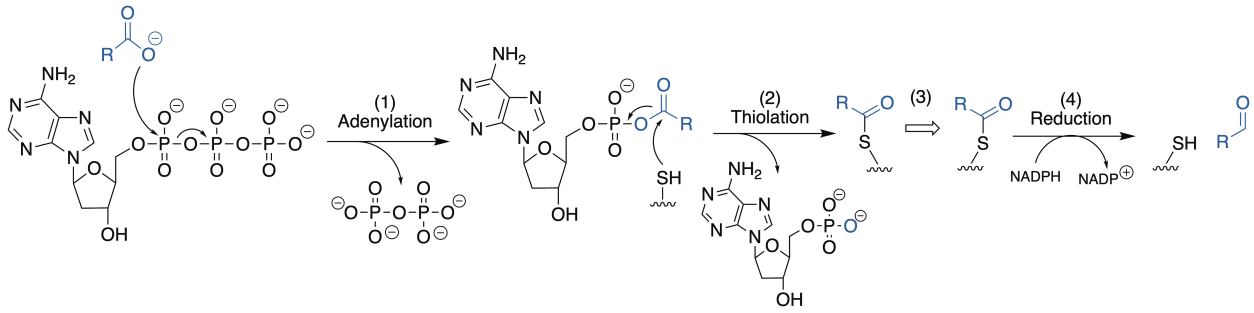

Figure 2-2: The proposed mechanism for CAR. The reaction initiates when an ATP and a carbocyclic acid enter the adenylation domain. (1) Adenylation: Carboxylic acid is deprotonated and serves as a nucleophile to nucleophilically attack the α-phosphate of ATP to form an AMP-acyl phosphoester. This is followed by the release of pyrophosphate. (2) Thiolation: The thiol group of the phosphopantetheine arm in the thiolation domain nucleophilically attacks the carbonyl carbon of the AMP-acyl phosphoester intermediate and releases AMP. After the acyl thioester is covalently bonded to the phosphopantetheine arm, (3) the phosphopantetheine arm transfers to the reduction domain. (4) Reduction: the NADPH reduces the thioester bond and releases the aldehyde product. Meanwhile, it regenerates the phosphopantetheine thiol group and produces $NADP^+$. [59]

In this chapter, *mm*CAR was transformed and expressed. The kinetics of *mm*CAR on three substrates were measured. Based on the kinetic activity results, the substrate–enzyme relation of *mm*CAR and PFOA was further investigated through a titration experiment. This study aimed to investigate the enzyme activity of *mm*CAR on PFOA, which is the first step of the proposed degradation of PFOA. In addition, this chapter explored the enzyme promiscuity of *mm*CAR.

2.2 MATERIALS AND METHODS

2.2.1 Plasmid transformation and protein production

Plasmid ordered from Twist Biosciences was transformed into BL21(DE3) *E.coli* through heat shock in a 42ºC water bath. Then, 200 µL of Terrific Broth (TB) was added, and the mixture was shaken at 37ºC for 1 hour. The cells wwere then plated onto a Lysogeny Broth (LB) agarose plate with kanamycin selection. The plate was incubated at 37ºC overnight. A single colony was selected to start a 3 mL culture with 1 mM kanamycin and shaken at 37ºC overnight. A total of 1 mL overnight culture was inoculated into a 500 mL TB sub-culture containing 1 mM kanamycin and 1 mM $MgSO_4$. The sub-culture was then incubated at 37ºC overnight. After incubation, the sub-culture was pelleted by being centrifuged at 4,700 rpm for 10 minutes. The cell pellet was resuspended in 500 mL induction TB media with 1x 5052, 1x NPS, 1 mM kanamycin, and 1 mM $MgSO_4$. The induction media was incubated at 18ºC for 24 hours, and the cell pellet was collected by centrifuging at 4,700 rpm for 10 minutes. The collected cell pellets were resuspended in 25 mL wash buffer (50 mM Hepes (pH 7.5), 200 mM NaCl, 10 mM imidazole) before being frozen at -20ºC.

2.2.2 Protein purification

After thawing the resuspended cell pellet, 1 mL of lysis buffer (1 mM DNase, 1 mM PMSF, 1 mM lysozyme) was added before using sonication to lyse the cells. Sonication was set with an amplitude of 60 Hz with the power on for 30 seconds, then off for 30 seconds, repeatedly for 2 minutes. The lysis cell pellet and liquid lysate were separated by centrifugation at 12,000 x g for 45 minutes. The lysate was then transferred into a 15 mL immobilized metal ion chromatography column loaded with 1 mL of 50% Ni-NTA resin slurry. Once the lysate flowed through, 15 mL of wash buffer (50 mM Hepes, 200 mM NaCl, 10 mM Imidazole) was added five times to wash the

bed of the beads. The protein could be eluted with 1.4 mL wash buffer with 200 mM imidazole after all the wash went through the column. The final concentration of the protein was determined by absorbance at 280 nm (A280), and the purity of the protein was verified by sodium dodecyl sulfate-polyacrylamide gel electrophoresis (SDS-PAGE).

2.2.3 Carboxylic acid reductase kinetic assay

The purified enzyme was diluted to 0.6 mg/mL and assayed against three substrates: benzoic acid, octanoic acid, and PFOA (Figure 2-3). All substrates were prepared in 100 mM in 50% DMSO (v/v), which was used to dilute the substrates in PCR tubes. The concentration ranged from 100 mM to 0.1 mM. Then, 10 mL reaction mixture was made as follows: 100 mM Tris-HCl (pH=7.5), 1 mM ATP, 0.25 mM NADPH, 10 mM $MgCl_2$. The reaction mix was prepared fresh and kept on ice. Ten microliters of purified enzyme and 80 µL of reaction mix were pipetted into a 96-well assay plate. Ten microliters of the substrates were added using a multichannel pipet to initiate the reaction. Green fluorescent protein (GFP) was used as a negative control in all assays. The reaction was monitored at room temperature for 1 hour. The enzyme activity of *mm*CAR against different substrates was monitored in the spectrometer at 340 nm, corresponding to the reduction of the NADPH cofactor. All assays were tested in duplicate. The kinetic parameters were obtained by calculating the initial velocity (v_0) of the enzyme reaction using the Data Reduction function on Gen5^{TM} 2.09, and data was fitted into the Michaelis-Menten equation. [37]

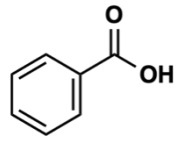	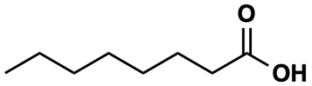	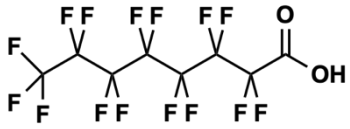
Benzoic acid	Octanoic acid	Perfluorooctanoic acid (PFOA)

Figure 2-3: Substrates that were tested with *mm*CAR.

2.2.4 Perfluorooctanoic acid titration Assay

An experiment of PFOA titration was performed to examine the substrate–enzyme relationship. The assay was performed the same day as protein purification. The enzyme was diluted to 1 mg/mL using wash buffer. Three different concentrations of PFOA (1 mM, 0.1 mM, 0.01, and 0.001 mM) were dissolved in 50% DMSO and incubated with reaction buffer (100 mM Tris-HCl (pH=7.5), 1 mM ATP, 0.25 mM NADPH, 10 mM $MgCl_2$) at room temperature for 20 minutes. To initiate the reactions, 10 mM of benzoic acid was added into the mixture. The enzyme reaction was monitored on the spectrometer at 340 nm. The duration of the reaction was 1 hour at room temperature. The positive control for this experiment was 10 mM benzoic acid, and the negative control was 1 mM PFOA.

2.3 RESULTS AND DISCUSSION

2.3.1 Yield of Carboxylic Acid Reductase and SDS-PAGE

The protein yield of *mm*CAR and GFP was 3.3 mg/mL and 3.5 mg/mL, respectively (see gel image in Figure 2-4). Based on the SDS-PAGE results, the dominant band at 130 kD represents CAR, verifying that over 80% of the elution protein mixture was the targeted enzyme. Another dominant band at 27 kD represents GFP and shows that the protein production process was efficient. Ni-NTA is a widely used metal ion in protein purification. It can efficiently bind to His-tag protein, but it can also bind nonspecifically to other proteins with histidine clusters. This could explain why there were many nonspecific protein bands visible on the gel. Nonspecific protein bands can be eliminated by increasing the imidazole concentration in the wash buffer or increasing the number of washes. However, this strategy can potentially cause a loss of the target protein too. In addition, using a more binding specific resin, such as cobalt resin slurry, can potentially increase final protein purity.

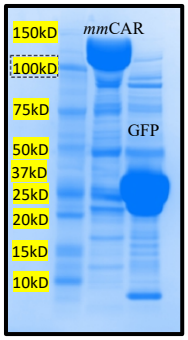

Figure 2-4: The purified protein's yield visualized on an SDS-PAGE gel. The protein concentrations were obtained from the absorbance reading at 280 nm, which are 3.3 mg/mL and 3.5 mg/mL for *mm*CAR and GFP, respectively.

2.3.2 Michaelis–Menten Kinetics of *mm*CAR against Different Substrates.

In this study, *mm*CAR was exposed to three different substrates, benzoic acid, octanoic acid, and PFOA, to determine its enzyme kinetics using Michaelis–Menten plots. Absorbances at 340 nm were monitored throughout the entire reaction time. The Michaelis–Menten plots are shown in Figure 2-5. The x-axis and y-axis represent the substrate concentration and reaction rate. The k_{cat} and K_M values for each substrate were calculated from the Lineweaver–Burk Plots, which were obtained by taking the reciprocal of Michaelis–Menten equations. The calculated k_{cat}, K_M, and k_{cat} / K_M are summarized in Table (2-1).

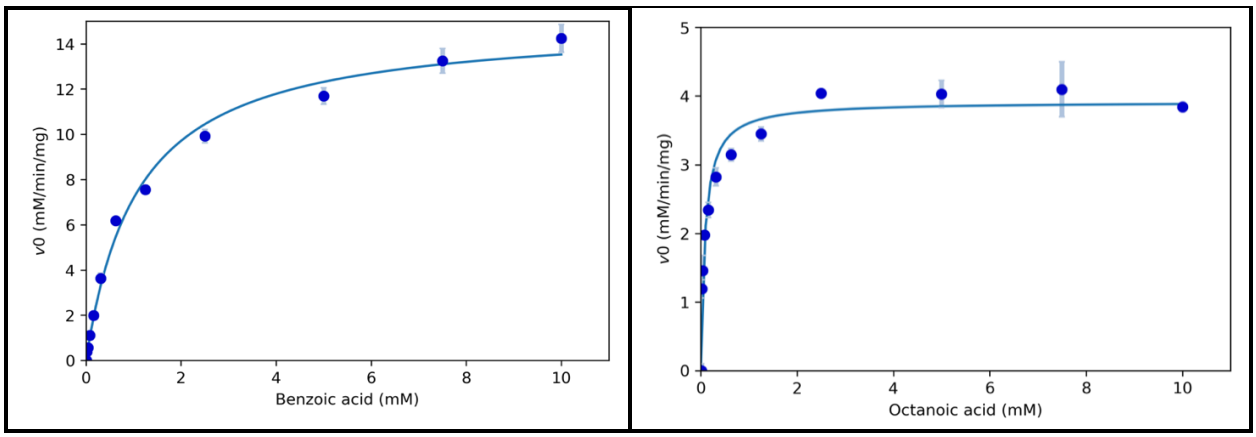

Figure 2-5: The Michaelis–Menten plots for *mm*CAR against benzoic acid and octanoic acid. There was no activity observed on *mm*CAR against PFOA. The error bars represent the standard deviation of two independent datasets.

Table 2-1: Kinetic parameters for CAR against benzoic acid, octanoic acid, and perfluorooctanoic acid (PFOA). The standard errors are the standard deviation of two independent measurements. ND: Not detected.

Substrate	k_{cat} (min^{-1})	K_M (mM)	k_{cat} / K_M ($min^{-1}mM^{-1}$)
Benzoic acid	149.5±54.3	0.5±0.3	303.6
Octanoic acid	57.5±0.6	0.04±0.008	1370.5
PFOA	ND	ND	ND

The enzyme concentration of *mm*CAR used in these assays was 0.06 mg/mL. This study hypothesized that *mm*CAR would be active on all three tested substrates. Benzoic acid is the native substrate for *mm*CAR. *mm*CAR showed activity on benzoic acid, validating that *mm*CAR was correctly expressed and function. Octanoic acid, used as a second positive control, has the same carbon length as PFOA. Compared to benzoic acid (303.6 $min^{-1}mM^{-1}$), *mm*CAR had higher catalytic efficiency than octanoic acid (1,370.5 $min^{-1}mM^{-1}$). These results agreed with a previous study, which suggested that a larger substrate could create more interaction in the enzyme binding pocket and therefore result in a smaller K_M. [59] Unfortunately, little to no enzyme activity was observed on *mm*CAR with PFOA (data not shown).

To determine whether *mm*CAR's activity on PFOA could be detected or improved, the enzyme concentration in the kinetic assay was increased, which decreased the possibility that the interaction between *mm*CAR and PFOA was below the detection limit of the spectrometer. Therefore, the kinetic assay for *mm*CAR and PFOA was repeated with a 3-fold higher enzyme concentration (0.3 mg/mL) than the previous experiment; however, no activity was observed (data not shown). It was also possible that *mm*CAR was not active on PFOA or was inhibited by PFOA. Based on the acid dissociation constant values of *mm*CAR, PFOA (pKa = -0.1) has lower pKa than octanoic acid (pKa = 4.89) and benzoic acid (pKa = 4.2). [60] The proton on the PFOA is easier to release in the neutral environment (pH=7.5) compare to benzoic acid. However, further

experiments are needed to validate if PFOA is a good electrophile or an acid for the first step (adenylation) of nucleophilic attack in the CAR catalytic mechanism.

2.3.3 Mechanism Validation through PFOA Titration

PFOA titration was performed to examine the relationship between PFOA and *mm*CAR (Figure 2-4). The real-time assay curves show that the rate of the reactions decreases (close to the positive control) with increasing concentrations of PFOA titrated into the reaction. This suggests that PFOA inhibited enzyme activity when its concentration ranged from 1 μM to 1 mM. After converting the enzyme concentration into molar concentration, there was 3 μM of *mm*CAR present in the assay. When the concentration of PFOA was higher than *mm*CAR, it was hypothesized that *mm*CAR was fully occupied by PFOA before the addition of benzoic acid. After benzoic acid was added, the results showed that *mm*CAR did not abolish all activity, and all reactions eventually reached the same rate. Therefore, this strongly suggested that PFOA potentially inhibited the enzyme activity through non-covalently binding to the enzyme active site, which interfered with the binding of benzoic acid. The reactive substrate (benzoic acid) needed to "beat" the non-covalent inhibitor (PFOA) to push the reaction forward, which decreased the reaction rate compared to the positive control; the reactions eventually reached the same rate since the concentration of benzoic acid was constant for all reaction. The carboxylic acid on the PFOA was potentially deprotonated in the neutral environment; however, the nucleophilic attack at the adenylation step did not occur. The catalytic reaction, therefore, did not continue. This result suggested that a charged group adjacent to the carboxylic acid would be a poor substrate for *mm*CAR, especially with the strong induction effect caused by fluorine. This would be consistence with highly electron-deficient substrates. In addition, the steric allowance of the CAR binding pocket is limited. [61]

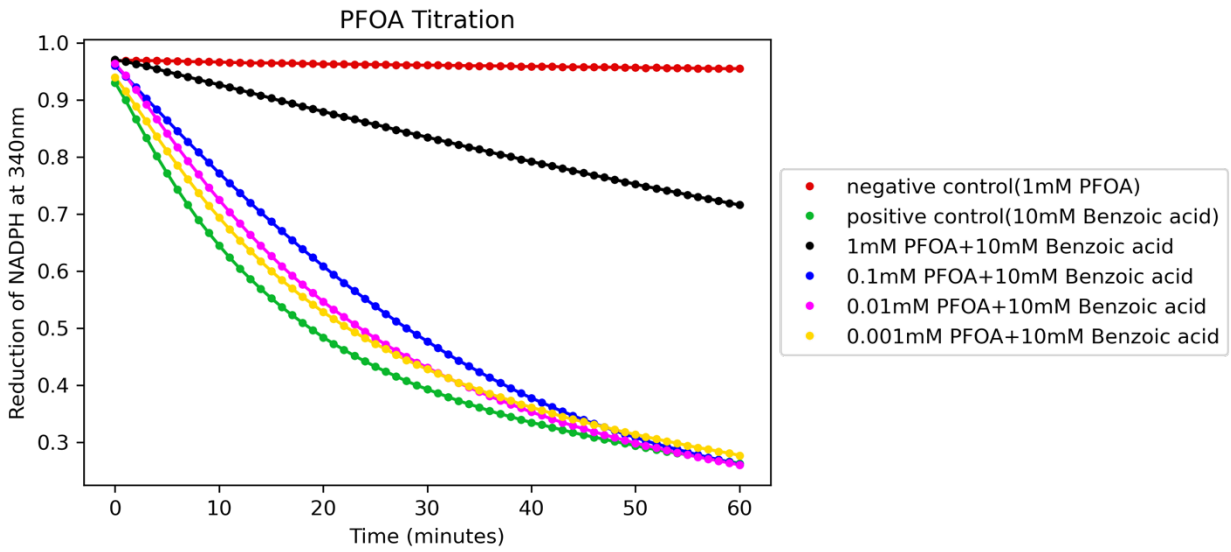

Figure 2-6: The inhibition of the reaction of *mm*CAR and 10 mM benzoic acid substrates by PFOA. Each dot represents a single measurement of the absorbance at 340 nm, which represents the reduction of NADPH. All dots are connected with lines. The internal for each data point is one minute and the reaction assay ran for 60 minutes. Red represents the negative control, and green represents the positive control. Black, blue, magenta, and gold represent 1 mM, 0.1 mM, 0.01 mM, and 0.001 mM of PFOA presented in the assay, respectively.

2.4 CONCLUSION AND RECOMMENDATION

In biofuel production, there is increasing interest in the reaction cascade of CAR and ADO. Expanding the application of this reaction cascade into the biodegradation of PFOA will be beneficial to sustainably and human health. Even though some methods have been shown to degrade PFOA successfully, these methods are not as accessible as biodegradation when applied on a larger scale. [[51,53]] Therefore, this study proposed a biodegradation pathway for PFOA through the CAR and ADO reaction cascade.

A CAR from *Mycobacterium marinum*, which showed enzyme activity on fatty acid substrates, was transformed, expressed, and assayed against three different substrates: benzoic acid, octanoic acid, and PFOA. The kinetic assay showed that the *mm*CAR was appropriately expressed. Unfortunately, *mm*CAR did not demonstrate activity on PFOA either under normal or modified assay conditions. Therefore, the enzyme–substrate relationship between *mm*CAR and PFOA was

further validated through a titration assay, which showed that PFOA acts as an inhibitor to *mm*CAR through reversible, non-covalent binding. This is because of the inherited chemical properties of PFOA, and would be similar observed on other electron deficient substrates. Although no *mm*CAR activity was observed on PFOA, this study provides the basis for an alternative biodegradation pathway for PFOA, which in the future, can be further modified through protein engineering.

CONCLUDING REMARKS

As biological catalysts, enzymes play an essential role in both the environment and human life. However, global climate change has changed the natural habitat of enzymes, causing enzyme activity loss. One major impact of enzyme activity loss is the loss of yield of wheat with the increasing temperatures; however, the demand for wheat has been increasing with the growing population. [14] Therefore, as suggested by Dr. Trick's research, Chapter 1 of this thesis focused on characterizing the thermostability of different crops and compared their thermostability to that of wheat. [15] The results showed that some SSSIs, such as *Vitvi*SSI, showed better heat resistance than wheat, which can be a candidate for designing or modifying the SSSIs of wheat in the future. Future studies should expand to characterize the thermostability of more SSSIs, especially those from crop plants grown in hot climates.

In addition to improving enzyme activity, we also explored a different aspect of enzyme application important to humans. With the increasing attention on PFOA pollutants in the environment, Chapter 2 investigated whether the *mm*CAR and ADO reaction cascade could biodegrade PFOA. Unfortunately, *mm*CAR could not catalyze PFOA; therefore, the *mm*CAR and ADO cascade reaction did not accomplish this objective. Interestingly, this study found that PFOA inhibited *mm*CAR activity through non-covalent bonding, which can be added to current studies on CAR promiscuity. Chapter 2 suggested a biodegradation pathway for PFOA, which future studies should investigate further through computational enzyme design. The strategies that used for these studies can also be implied in pharmaceutical chemistry for improving drug efficiency when expose to high temperatures or discovering drug 'promiscuous activity' that makes them become inhibitors for enzymes. [62,63]

REFERENCES

(1) Arnold, F. H. Directed Evolution: Bringing New Chemistry to Life. *Angewandte Chemie - International Edition* **2018**, *57* (16), 4143–4148. https://doi.org/10.1002/anie.201708408.

(2) Nguyen, V.; Wilson, C.; Hoemberger, M.; Stiller, J. B.; Agafonov, R. v.; Kutter, S.; English, J.; Theobald, D. L.; Kern, D. Evolutionary Drivers of Thermoadaptation in Enzyme Catalysis. *Science (1979)* **2017**, *355* (6322), 289–294. https://doi.org/10.1126/SCIENCE.AAH3717.

(3) Arnold, F. H.; Wintrode, P. L.; Miyazaki, K.; Gershenson, A. How Enzymes Adapt: Lessons from Directed Evolution. *Trends in Biochemical Sciences* **2001**, *26* (2), 100–106. https://doi.org/10.1016/S0968-0004(00)01755-2.

(4) *The evolution of mutation rates: separating causes from consequences*. https://onlinelibrary.wiley.com/doi/epdf/10.1002/1521-1878%28200012%2922%3A12%3C1057%3A%3AAID-BIES3%3E3.0.CO%3B2-W?saml_referrer (accessed 2022-07-04).

(5) Biotechnology Journal. **2014**. https://doi.org/10.1002/biot.201400150.

(6) Deckers, M.; Deforce, D.; Fraiture, M.-A.; Roosens, N. H. C. Genetically Modified Micro-Organisms for Industrial Food Enzyme Production: An Overview. https://doi.org/10.3390/foods9030326.

(7) Jestin, J. L.; Vichier-Guerre, S. How to Broaden Enzyme Substrate Specificity: Strategies, Implications and Applications. *Research in Microbiology* **2005**, *156* (10), 961–966. https://doi.org/10.1016/J.RESMIC.2005.09.004.

(8) Polizzi, K. M.; Bommarius, A. S.; Broering, J. M.; Chaparro-Riggers, J. F. Stability of Biocatalysts. *Current Opinion in Chemical Biology* **2007**, *11* (2), 220–225. https://doi.org/10.1016/J.CBPA.2007.01.685.

(9) Glasner, M. E.; Truong, D. P.; Morse, B. C.; Glasner, M. E. How Enzyme Promiscuity and Horizontal Gene Transfer Contribute to Metabolic Innovation. https://doi.org/10.1111/febs.15185.

(10) Nobeli, I.; Favia, A. D.; Thornton, J. M. Protein Promiscuity and Its Implications for Biotechnology. https://doi.org/10.1038/nbt1519.

(11) O'Brien, P. J.; Herschlag, D. Catalytic Promiscuity and the Evolution of New Enzymatic Activities. *Chemistry and Biology* **1999**, *6* (4). https://doi.org/10.1016/S1074-5521(99)80033-7.

(12) Hult, K.; Berglund, P. Enzyme Promiscuity: Mechanism and Applications. *Trends in Biotechnology* **2007**, *25* (5), 231–238. https://doi.org/10.1016/J.TIBTECH.2007.03.002.

(13) Giraldo, P.; Benavente, E.; Manzano-Agugliaro, F.; Gimenez, E. Worldwide Research Trends on Wheat and Barley: A Bibliometric Comparative Analysis. https://doi.org/10.3390/agronomy9070352.

(14) Jenner, C.; Denyer, K.; Guerin, J. Thermal Characteristics of Soluble Starch Synthase From Wheat Endosperm. *Functional Plant Biology* **1995**, *22* (4), 703–709. https://doi.org/10.1071/PP9950703.

(15) Tian, B.; Talukder, S. K.; Fu, J.; Fritz, A. K.; Trick, H. N. Expression of a Rice Soluble Starch Synthase Gene in Transgenic Wheat Improves the Grain Yield under Heat Stress Conditions. https://doi.org/10.1007/s11627-018-9893-2.

(16) Wardlaw, I. I. F.; Dawson, I. A.; Munibi, P.; Fewster, R. The Tolerance of Wheat to High Temperatures during Reproductive Growth. I Survey Procedures and General Response Patterns. *Aust. J. Agric. Res* **1989**, *40*, 1–13.
(17) Talukder, A. S. M. H. M.; McDonald, G. K.; Gill, G. S. Effect of Short-Term Heat Stress Prior to Flowering and Early Grain Set on the Grain Yield of Wheat. *Field Crops Research* **2014**, *160*, 54–63. https://doi.org/10.1016/J.FCR.2014.01.013.
(18) Buléon, A.; Colonna, P.; Planchot, V.; Ball, S. Starch Granules: Structure and Biosynthesis. *International Journal of Biological Macromolecules* **1998**, *23* (2), 85–112. https://doi.org/10.1016/S0141-8130(98)00040-3.
(19) Mua, J. P.; Jackson, D. S. *Fine Structure of Corn Amylose and Amylopectin Fractions with Various Molecular Weights †*; 1997.
(20) Coutinho, P. M.; Deleury, E.; Davies, G. J.; Henrissat, B. An Evolving Hierarchical Family Classification for Glycosyltransferases. *Journal of Molecular Biology* **2003**, *328* (2), 307–317. https://doi.org/10.1016/S0022-2836(03)00307-3.
(21) Jeon, J. S.; Ryoo, N.; Hahn, T. R.; Walia, H.; Nakamura, Y. Starch Biosynthesis in Cereal Endosperm. *Plant Physiology and Biochemistry* **2010**, *48* (6), 383–392. https://doi.org/10.1016/J.PLAPHY.2010.03.006.
(22) Cho, Y.-G.; Kang, K.-K. Plants Editorial Functional Analysis of Starch Metabolism in Plants. https://doi.org/10.3390/plants9091152.
(23) Cuesta-Seijo, J. A.; Nielsen, M. M.; Marri, L.; Tanaka, H.; Beeren, S. R.; Palcic, M. M. Structure of Starch Synthase i from Barley: Insight into Regulatory Mechanisms of Starch Synthase Activity. *Acta Crystallographica Section D: Biological Crystallography* **2013**, *69* (6), 1013–1025. https://doi.org/10.1107/S090744491300440X/HTTPS://JOURNALS.IUCR.ORG/SERVICES/RSS.HTML.
(24) Huang, B.; Keeling, P. L.; Hennen-Bierwagen, T. A.; Myers, A. M. Comparative in Vitro Analyses of Recombinant Maize Starch Synthases SSI, SSIIa, and SSIII Reveal Direct Regulatory Interactions and Thermosensitivity. *Archives of Biochemistry and Biophysics* **2016**, *596*, 63–72. https://doi.org/10.1016/J.ABB.2016.02.032.
(25) Commuri, P. D.; Keeling, P. L. *Chain-Length Speci®cities of Maize Starch Synthase I Enzyme: Studies of Glucan Af®nity and Catalytic Properties*.
(26) Fujita, N.; Yoshida, M.; Asakura, N.; Ohdan, T.; Miyao, A.; Hirochika, H.; Nakamura, Y. Function and Characterization of Starch Synthase I Using Mutants in Rice. https://doi.org/10.1104/pp.105.071845.
(27) Zahedi, M.; Sharma, R.; Jenner, C. F. Effects of High Temperature on Grain Growth and on the Metabolites and Enzymes in the Starch-Synthesis Pathway in the Grains of Two Wheat Cultivars Differing in Their Responses to Temperature. *Functional Plant Biology* **2003**, *30*, 291–300. https://doi.org/10.1071/FP02205.
(28) Rijven, A. H. G. C. *Heat Inactivation of Starch Synthase in Wheat Endosperm Tissue*; 1986; Vol. 81.
(29) Keeling, P. L.; Bacon, P. J.; Holt, D. C. *Elevated Temperature Reduces Starch Deposition in Wheat Endosperm by Reducing the Activity of Soluble Starch Synthase*; Springer-Verlag, 1993; Vol. 191.
(30) Ehlers, J. D.; Hall, A. E. Cowpea (Vigna Unguiculata L. Walp.). *Field Crops Research* **1997**, *53* (1–3), 187–204. https://doi.org/10.1016/S0378-4290(97)00031-2.

(31) Gibson, D. G.; Young, L.; Chuang, R.-Y.; Craig Venter, J.; Hutchison III, C. A.; Smith, H. O. RECEIVED 5 JANUARY; ACCEPTED 16 MARCH; PUBLISHED ONLINE 12. *NATURE METHODS* **2009**, *6* (5). https://doi.org/10.1038/NMETH.1318.
(32) Sanger, F.; Nicklen, S.; Coulson, A. R. *DNA Sequencing with Chain-Terminating Inhibitors (DNA Polymerase/Nucleotide Sequences/Bacteriophage 4X174)*; 1977; Vol. 74.
(33) *Geneious | Bioinformatics Software for Sequence Data Analysis*. https://www.geneious.com/ (accessed 2022-07-06).
(34) Studier, F. W. Protein Production by Auto-Induction in High-Density Shaking Cultures. **2005**. https://doi.org/10.1016/j.pep.2005.01.016.
(35) Sreenath, H. K.; Bingman, C. A.; Buchan, B. W.; Seder, K. D.; Burns, B. T.; Geetha, H. v.; Jeon, W. B.; Vojtik, F. C.; Aceti, D. J.; Frederick, R. O.; Phillips, G. N.; Fox, B. G. Protocols for Production of Selenomethionine-Labeled Proteins in 2-L Polyethylene Terephthalate Bottles Using Auto-Induction Medium. *Protein Expression and Purification* **2005**, *40* (2), 256–267. https://doi.org/10.1016/J.PEP.2004.12.022.
(36) Gosselin, S.; Alhussaini, M.; Streiff, M. H.; Takabayashi, K.; Palcic, M. M. A Continuous Spectrophotometric Assay for Glycosyltransferases. *Analytical Biochemistry* **1994**, *220* (1), 92–97. https://doi.org/10.1006/ABIO.1994.1303.
(37) *Microplate Software: BioTek Gen5 Data Analysis Software*. https://www.biotek.com/products/software-robotics-software/gen5-microplate-reader-and-imager-software/related-products/ (accessed 2022-07-18).
(38) *ExPASy - Compute pI/Mw tool*. https://web.expasy.org/compute_pi/ (accessed 2022-07-27).
(39) Lasanta, C.; Caro, I.; Gómez, J.; Pérez, L. The Influence of Ripeness Grade on the Composition of Musts and Wines from Vitis Vinifera Cv. Tempranillo Grown in a Warm Climate. *Food Research International* **2014**, *64*, 432–438. https://doi.org/10.1016/J.FOODRES.2014.07.039.
(40) Analysis of Protein Complexes in Wheat Amyloplasts Reveals Functional Interactions among Starch Biosynthetic Enzymes 1[C][W][OA]. *Plant Physiology* **2008**, *146*, 1878–1891. https://doi.org/10.1104/pp.108.116244.
(41) Gahloth, D.; Dunstan, M. S.; Quaglia, D.; Klumbys, E.; Lockhart-Cairns, M. P.; Hill, A. M.; Derrington, S. R.; Scrutton, N. S.; Turner, N. J.; Leys, D. Structures of Carboxylic Acid Reductase Reveal Domain Dynamics Underlying Catalysis. *Nat Chem Biol* **2017**, *13* (9), 975–981. https://doi.org/10.1038/NCHEMBIO.2434.
(42) Derrington, S. R.; Turner, N. J.; France, S. P. Carboxylic Acid Reductases (CARs): An Industrial Perspective. *Journal of Biotechnology* **2019**, *304*, 78–88. https://doi.org/10.1016/J.JBIOTEC.2019.08.010.
(43) Kalim Akhtara, M.; Turner, N. J.; Jones, P. R. Carboxylic Acid Reductase Is a Versatile Enzyme for the Conversion of Fatty Acids into Fuels and Chemical Commodities. *Proc Natl Acad Sci U S A* **2013**, *110* (1), 87–92. https://doi.org/10.1073/PNAS.1216516110.
(44) Cutlan, R.; de Rose, S.; Isupov, M. N.; Littlechild, J. A.; Harmer, N. J. Using Enzyme Cascades in Biocatalysis: Highlight on Transaminases and Carboxylic Acid Reductases. *Biochimica et Biophysica Acta (BBA) - Proteins and Proteomics* **2020**, *1868* (2), 140322. https://doi.org/10.1016/J.BBAPAP.2019.140322.
(45) Aukema, K. G.; Makris, T. M.; Stoian, S. A.; Richman, J. E.; Münck, E.; Lipscomb, J. D.; Wackett, L. P. Cyanobacterial Aldehyde Deformylase Oxygenation of Aldehydes Yields n

- 1 Aldehydes and Alcohols in Addition to Alkanes. *ACS Catalysis* **2013**, *3* (10), 2228–2238. https://doi.org/10.1021/CS400484M/SUPPL_FILE/CS400484M_SI_001.PDF.
(46) Kallio, P.; Pásztor, A.; Thiel, K.; Akhtar, M. K.; Jones, P. R. An Engineered Pathway for the Biosynthesis of Renewable Propane. *Nature Communications 2014 5:1* **2014**, *5* (1), 1–8. https://doi.org/10.1038/ncomms5731.
(47) Xiao, F.; Simcik, M. F.; Halbach, T. R.; Gulliver, J. S. Perfluorooctane Sulfonate (PFOS) and Perfluorooctanoate (PFOA) in Soils and Groundwater of a U.S. Metropolitan Area: Migration and Implications for Human Exposure. *Water Research* **2015**, *72*, 64–74. https://doi.org/10.1016/J.WATRES.2014.09.052.
(48) Liu, Z.; Lu, Y.; Wang, P.; Wang, T.; Liu, S.; Johnson, A. C.; Sweetman, A. J.; Baninla, Y. Pollution Pathways and Release Estimation of Perfluorooctane Sulfonate (PFOS) and Perfluorooctanoic Acid (PFOA) in Central and Eastern China. *Science of The Total Environment* **2017**, *580*, 1247–1256. https://doi.org/10.1016/J.SCITOTENV.2016.12.085.
(49) Hu, J.; Yu, J.; Tanaka, S.; Fujii, S. Perfluorooctane Sulfonate (PFOS) and Perfluorooctanoic Acid (PFOA) in Water Environment of Singapore. https://doi.org/10.1007/s11270-010-0525-7.
(50) Butenhoff, J. L.; Olsen, G. W.; Pfahles-Hutchens, A. The Applicability of Biomonitoring Data for Perfluorooctanesulfonate to the Environmental Public Health Continuum. *Environmental Health Perspectives* **2006**, *114* (11), 1776–1782. https://doi.org/10.1289/EHP.9060.
(51) Lau, C.; Anitole, K.; Hodes, C.; Lai, D.; Pfahles-Hutchens, A.; Seed, J. REVIEW Perfluoroalkyl Acids: A Review of Monitoring and Toxicological Findings. *TOXICOLOGICAL SCIENCES* **2007**, *99* (2), 366–394. https://doi.org/10.1093/toxsci/kfm128.
(52) Fragki, S.; Dirven, H.; Fletcher, T.; Grasl-Kraupp, B.; Bjerve Gützkow, K.; Hoogenboom, R.; Kersten, S.; Lindeman, B.; Louisse, J.; Peijnenburg, A.; Piersma, A. H.; Princen, H. M. G.; Uhl, M.; Westerhout, J.; Zeilmaker, M. J.; Luijten, M. Systemic PFOS and PFOA Exposure and Disturbed Lipid Homeostasis in Humans: What Do We Know and What Not? *Critical Reviews in Toxicology* **2021**, *51* (2), 141–164. https://doi.org/10.1080/10408444.2021.1888073/SUPPL_FILE/ITXC_A_1888073_SM6618.XLSX.
(53) Shahsavari, E.; Rouch, D.; Khudur, L. S.; Thomas, D.; Aburto-Medina, A.; Ball, A. S. Challenges and Current Status of the Biological Treatment of PFAS-Contaminated Soils. *Frontiers in Bioengineering and Biotechnology* **2021**, *8*, 1493. https://doi.org/10.3389/FBIOE.2020.602040/BIBTEX.
(54) Verma, S.; Mezgebe, B.; Sahle-Demessie, E.; Nadagouda, M. N. Photooxidative Decomposition and Defluorination of Perfluorooctanoic Acid (PFOA) Using an Innovative Technology of UV-Vis/Zn x Cu 1-x Fe 2 O 4/Oxalic Acid. *Chemosphere* **2021**, *280*. https://doi.org/10.1016/J.CHEMOSPHERE.2021.130660.
(55) Wu, D.; Li, X.; Tang, Y.; Lu, P.; Chen, W.; Xu, X.; Li, L. Mechanism Insight of PFOA Degradation by ZnO Assisted-Photocatalytic Ozonation: Efficiency and Intermediates. *Chemosphere* **2017**, *180*, 247–252. https://doi.org/10.1016/J.CHEMOSPHERE.2017.03.127.
(56) Huang, S.; Jaffé, P. R. Defluorination of Perfluorooctanoic Acid (PFOA) and Perfluorooctane Sulfonate (PFOS) by Acidimicrobium Sp. Strain A6. *Environmental Science and Technology* **2019**.

https://doi.org/10.1021/ACS.EST.9B04047/ASSET/IMAGES/LARGE/ES9B04047_0002.JPEG.
(57) Liou, J. S. C.; Szostek, B.; DeRito, C. M.; Madsen, E. L. Investigating the Biodegradability of Perfluorooctanoic Acid. *Chemosphere* **2010**, *80* (2), 176–183. https://doi.org/10.1016/J.CHEMOSPHERE.2010.03.009.
(58) Wackett, L. P.; Robinson, S. L. The Ever-Expanding Limits of Enzyme Catalysis and Biodegradation: Polyaromatic, Polychlorinated, Polyfluorinated, and Polymeric Compounds. *Biochemical Journal* **2020**, *477* (15), 2875. https://doi.org/10.1042/BCJ20190720.
(59) Finnigan, W.; Thomas, A.; Cromar, H.; Gough, B.; Snajdrova, R.; Adams, J. P.; Littlechild, J. A.; Harmer, N. J. Characterization of Carboxylic Acid Reductases as Enzymes in the Toolbox for Synthetic Chemistry. *ChemCatChem* **2017**, *9* (6), 1005–1017. https://doi.org/10.1002/CCTC.201601249.
(60) Goss, K. U. The PKa Values of PFOA and Other Highly Fluorinated Carboxylic Acids. *Environmental Science and Technology* **2008**, *42* (2), 456–458. https://doi.org/10.1021/ES702192C/ASSET/IMAGES/LARGE/ES-2007-02192C_0001.JPEG.
(61) Moura, M.; Pertusi, D.; Lenzini, S.; Bhan, N.; Broadbelt, L. J.; Tyo, K. E. J. Characterizing and Predicting Carboxylic Acid Reductase Activity for Diversifying Bioaldehyde Production. https://doi.org/10.1002/bit.25860/abstract.
(62) Asial, I.; Cheng, Y. X.; Engman, H.; Dollhopf, M.; Wu, B.; Nordlund, P.; Cornvik, T. ARTICLE Engineering Protein Thermostability Using a Generic Activity-Independent Biophysical Screen inside the Cell. **2013**. https://doi.org/10.1038/ncomms3901.
(63) Seidler, J.; Mcgovern, S. L.; Doman, T. N.; Shoichet, B. K. Identification and Prediction of Promiscuous Aggregating Inhibitors among Known Drugs. **2003**. https://doi.org/10.1021/jm030191r.